Available online at www.sciencedirect.com
SCIENCE DIRECT®
Continental Shelf Research 25 (2005) 397–417
CONTINENTAL SHELF RESEARCH
www.elsevier.com/locate/csr

Local wind forcing of the Monterey Bay area inner shelf

Patrick T. Drake[a,*], Margaret A. McManus[b], Curt D. Storlazzi[c]

[a]*Long Marine Lab., University of California, Santa Cruz, CA, USA*
[b]*Department of Oceanography, University of Hawaii at Manoa, Honolulu, HI, USA*
[c]*US Geological Survey, Coastal and Marine Geology Program, Pacific Science Center, Santa Cruz, CA, USA*

Received 18 June 2003; received in revised form 16 September 2004; accepted 1 October 2004

Abstract

Wind forcing and the seasonal cycles of temperature and currents were investigated on the inner shelf of the Monterey Bay area of the California coast for 460 days, from June 2001 to September 2002. Temperature measurements spanned an approximate 100 km stretch of coastline from a bluff just north of Monterey Bay south to Point Sur. Inner shelf currents were measured at two sites near the bay's northern shore. Seasonal temperature variations were consistent with previous observations from the central California shelf. During the spring, summer and fall, a seasonal mean alongshore current was observed flowing northwestward in the northern bay, in direct opposition to a southeastward wind stress. A barotropic alongshore pressure gradient, potentially driving the northwestward flow, was needed to balance the alongshore momentum equation. With the exception of the winter season, vertical profiles of mean cross-shore currents were consistent with two-dimensional upwelling and existing observations from upwelling regions with poleward subsurface flow. At periods of 15–60 days, temperature fluctuations were coherent both throughout the domain and with the regional wind field. Remote wind forcing was minimal. During the spring upwelling season, alongshore currents and temperatures in the northern bay were most coherent with winds measured at a nearby land meteorological station. This wind site showed relatively low correlations to offshore buoy wind stations, indicating localized wind effects are important to the circulation along this stretch of Monterey Bay's inner shelf.

Keywords: Coastal upwelling; Inner shelf; Wind-driven currents; Ekman transport

1. Introduction

The inner continental shelf, defined here as water depths shoreward of 30 m, plays a critical role in both coastal circulation and the dynamics of marine ecosystems. Measurements show wind-driven upwelling on the US west coast, which

*Corresponding author. Long Marine Laboratory, University of California, Santa Cruz, 100 Shaffer Road, Santa Cruz, California 95060, USA.
E-mail address: drake@biology.ucsc.edu (P.T. Drake).

0278-4343/$ - see front matter © 2004 Elsevier Ltd. All rights reserved.
doi:10.1016/j.csr.2004.10.006

eventually feeds the elevated biological productivity found there, will be strongest over the inner shelf, closest to the shore (Huyer, 1983; Winant et al., 1987). These measurements are consistent with theoretical treatments of coastal upwelling (Allen, 1975), which predict that upwelling will be most pronounced within the baroclinic Rossby radius of the coast, roughly within 10 km of the shoreline. Satellite images (Kosro et al., 1991) reveal the importance of upwelling on the inner shelf to the growth of the larger-scale upwelling front and coastal transition zone further offshore.

To gain a better understanding of the upwelling and wind forcing on the inner shelf, long-term temperature and current measurements made in the Monterey Bay region of the US west coast were studied and compared to a variety of wind measurements. The observations and analysis summarized here were performed at the University of California, Santa Cruz, and were supported by the Partnership for Interdisciplinary Studies of Coastal Oceans (PISCO), a multi-institutional research program. Observations spanned well over 1 year, from 4 June 2001 to 7 September 2002. The spatial extent of the study was approximately 100 km, from a bluff just north of Monterey Bay south to Point Sur.

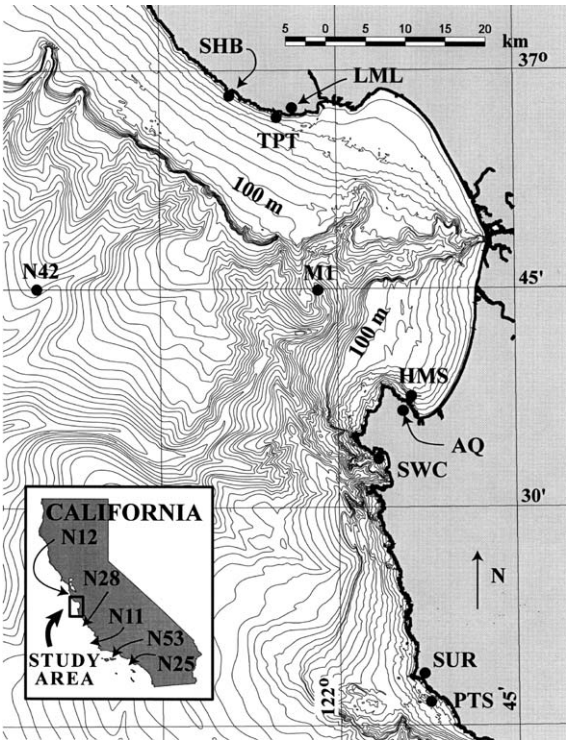

Fig. 1. Study site showing the Monterey Bay area of the California coast and locations of wind stations (N12, LML, N42, M1, AQ, SUR, N28, N11, N53, N25), temperature moorings (SHB, TPT, M1, HMS, SWC, PTS) and ADCP current profilers (SHB, TPT). Water depth of the PISCO inner shelf stations (SHB, TPT, HMS, SWC, PTS) was ~20 m. Isobath contour interval is 10 m for water depths <200 m and 100 m for depths >200 m.

2. Methods

2.1. Instrumentation

The study encompassed five inner shelf moorings north of, inside, and to the south of Monterey Bay (Fig. 1, Table 1). Located in an approximate water depth of 20 m, all five shelf moorings measured temperature at three depths, referred to as bottom, middle, and top. Currents, measured with Acoustic Doppler Current Profilers (ADCPs), were also analyzed at the two northernmost sites (SHB and TPT). All inner shelf moorings were maintained by the UCSC PISCO program. Supplementary temperature data from a deep-water mooring inside Monterey Bay (M1) and a variety of wind data sets were also used to complement the analysis. Maintained by the Monterey Bay Aquarium Research Institute (MBARI), the M1 mooring is located in a nominal water depth of 1600 m in the heart of the Monterey Submarine Canyon. Only temperature from M1's 10 m depth will be presented here, as this depth was available for both calendar years. Wind data from 10 different sites were employed in the analysis (Table 2). Both land (LML, AQ, SUR) and offshore buoy wind stations, including M1, were used. All buoy wind stations, with the exception of M1, were maintained by the National Data Buoy Center. Land-based wind measurements were made available from the Monterey Bay Aquarium (AQ), UCSC's Long Marine Lab (LML) and the Department of Meteorology at the Naval Postgraduate School, which maintains a meteorological station at the Point Sur Naval Station (SUR).

Table 1
Mooring locations and instrument depths

Name	ID	Water depth (m)	Lat., °N	Lon., °W	Thermistor depths (m)	ADCP range[a]	Major (y-) axis (°T)
Sand Hill Bluff	SHB	20	36.97	122.16	3, 11, 19	2–17	327
Terrace Point	TPT	18	36.94	122.08	4, 10, 17	3–15	295
M1	M1	1600	36.75	122.03	10	—	—
Hopkins Marine Station	HMS	18	36.62	121.90	3, 10, 17	—	—
Stillwater Cove	SWC	21	36.56	121.94	5, 12, 20	—	—
Point Sur	PTS	20	36.28	121.87	4, 10, 18	—	—

All depths in meters below MLLW. See Fig. 1 for site locations.
[a]Refers to valid measurement depths for upward-looking ADCPs.

Table 2
Wind measurement stations

Station name	ID	Lat., °N	Lon., °W	Major (y) axis (°T)	y (km)[a]
NDBC Buoy 46012, Half Moon Bay	N12	37.36	122.88	333	85
Long Marine Lab	LML	36.95	122.07	282	25
NDBC Buoy 46042, Monterey Bay	N42	36.75	122.42	317	0
M1 Buoy, Monterey Bay	M1	36.75	122.03	315	0
Monterey Bay Aquarium	AQ	36.62	121.90	308	−20
Point Sur Naval Station	SUR	36.30	121.89	334	−70
NDBC Buoy 46028, Cape San Martin	N28	35.74	121.89	315	−135
NDBC Buoy 46011, Santa Maria	N11	34.88	120.87	326	−280
NDBC Buoy 46053, Santa Barbara East	N53	34.24	119.85	278	−420
NDBC Buoy 46025, Santa Monica Basin	N25	33.75	119.08	293	−510

[a]Refers to approximate alongshore distance relative to N42. Distances were estimated roughly from NOAA nautical charts.

Temperatures at the inner shelf sites were measured with Onset StowAway-XTI temperature loggers. The Onset sensors have a precision of ~0.2 °C. Velocities were measured with bottom-mounted, upward-looking RD Instruments 600 kHz Workhorse Sentinel ADCPs. The vertical resolution of the ADCP was 1 m at all sites. The nominal uncertainty in the ADCP hourly measurements due to Doppler noise was ~0.2 cm/s. Thermistor depths and the valid ADCP range for each site are shown in Table 1. ADCP depths refer to bin centers.

2.2. Data selection and processing

The overall time period selected for study was chosen for its comprehensive wind, ADCP and temperature data coverage. Using the oceanographic "seasons" identified by Largier et al. (1993) for the northern California coast, the study period was further divided into four separate subperiods for statistical analysis (Table 3). These subperiods correspond to the spring upwelling season, the fall relaxation season, the winter storm season and a complete year surrounding the three seasons. Each of the three seasons spans 108 days and was delineated based on the timing of the spring transition, seasonal temperature minimums and maximums, and the avoidance of data gaps. Throughout this study, calendar days are numbered consecutively, with day 0 starting 12 a.m. Pacific Standard Time 1 January 2000. Some data beyond the bounds of the study period (not presented for the sake of brevity) were used to

Table 3
Study sub-periods used in statistical analysis

Season or demarcation	Dates	Day numbers
2001–2002 year	20 July 2001–20 July 2002	566–931.25
Fall 2001, relaxation season	24 July 2001–9 November 2001	570–678
Winter 2001–2002, storm season	27 November 2001–15 March 2002	696–804
Spring 2002, upwelling season	31 March 2002–17 July 2002	820–928

help determine the timing of the seasonal maximums and minimums discussed in Section 3.1. In many ways, the data were consistent with previous observations on the California coast (Section 3.1.). However, it is emphasized here that these three 108-day seasons may not necessarily be generic representations of fall, winter, and springtime conditions in the area.

Except for use in the Richardson number calculation (Section 3.1.), all data were hourly averaged and low-passed filtered (half-power period of 36 h). When possible, data gaps were filled with linear regressions from significantly correlated sensors on common moorings. Large record gaps of the deepest ADCP bin at both SHB and TPT (the bin occasionally failed due to a firmware problem) were filled using a regression from a neighboring bin. A 44-day gap in PTS bottom temperature during spring 2002 and a 15-day gap in HMS top temperature during fall of 2001 were filled with a linear regression from their respective moorings' middle sensors. However, most gaps were smaller (<2 days) and could not be filled with regressions from neighboring sensors. The remaining gaps were filled with low-passed white noise with the same mean and low-passed variance as the surrounding season or year. The data set contained only one substantial gap filled with noise: a 16-day gap in SHB current in fall 2001. Unless explicitly stated otherwise, all statistical calculations refer to the time periods in Table 3, with the data low-passed and gaps filled as described above.

The principal axes (Kundu and Allen, 1976) were determined for both winds and depth-averaged currents, and the major axes are listed in Tables 1 and 2. The calculation was based on the entire year, 20 July 2001–20 July 2002 (365.25 days), surrounding the three seasons. The directions in Tables 1 and 2 define the positive y-axis (alongshore) for both winds and currents. This gives the positive alongshore direction as roughly northwestward at all sites. Correspondingly, the positive x-axis points roughly northeastward (onshore) at all sites. The major axes of the currents and winds generally followed the isobaths, as would be expected from topographic steering close to the coastline and coastal mountains.

A linear trend was removed from all data before making standard deviation and correlation calculations. Effective degrees of freedom for correlation significance levels were determined using the integral time scale of the data, as suggested by Emery and Thomson (1997, Chapter 3), and were calculated by integrating the autocorrelation out to the first zero-crossing. All coherence calculations were made by subdividing the data into 60- or 18-day increments, removing a linear trend, multiplying by a Hanning window and block-averaging with a 50% overlap. Significance levels on the coherence estimates were determined using the Goodman formula (Thompson, 1979), with account made for averaging overlapping, correlated transforms as prescribed by Harris (1978). To keep the plots uncluttered error bars are not shown for the phase. The standard deviation of the phase varies inversely with the coherence (Bendat and Piersol, 2000, Chapter 9). To give some sense of the uncertainty in the phase estimates, when the coherence is significantly different from zero, the standard deviation of the phase is approximately 20° or less. Data for power spectra calculations were subdivided into three 54-day increments with 50% overlap, detrended, and multiplied by a Hanning window.

3. Results

3.1. General seasonality

Seasonal wind trends for N42 and LML (Figs. 2 and 3) were generally consistent with previous reported observations along the central California coast (Largier et al., 1993; Strub et al., 1987). Because of the interaction of large-scale atmospheric pressure systems (Lentz, 1987), winds are predominantly southeastward (equatorward) during spring, summer, and early fall (March–November in 2001 and 2002). This southeastward wind is episodically interrupted by brief relaxations lasting approximately 2–7 days, when the wind either weakens or turns northwestward. During the winter storm season, winds become more variable and their seasonal mean (108-day average) weakens. This can be seen both in the time history plots (Fig. 3) and basic statistics (Table 4a). Note the decrease in the mean and increase in the standard deviation for both LML and N42 during winter. The other wind sites in the Monterey Bay area, N12, M1, AQ, SUR, N28 (not shown), displayed a similar pattern of relatively strong southeastward winds during spring, summer and fall and a reduced mean in winter. During 2001 and 2002 at N42, monthly means of this southeastward wind peaked in June (monthly averages not shown). Regardless of season, the absolute magnitude of the wind was significantly less at the land stations LML and AQ compared to the NDBC buoys (Fig. 3). The wind velocities were not adjusted for differing sensor heights; this would have exaggerated the land/buoy difference, as the sensors were higher at the land stations. As discussed by Halliwell and Allen (1987), increased friction over land and/or the varying strength of the diurnal seabreeze/landbreeze with increasing distance from shore may be responsible for the effect.

Winds and currents were generally highly polarized along their respective major axes. The degree of polarization can be quantified with the ellipticity, defined here as major-axis-variance/minor-axis-variance. Ellipticities were typically well above 50 for currents and ranged from 4 to 12 for winds when calculated over the complete year. LML was an exception and showed the least

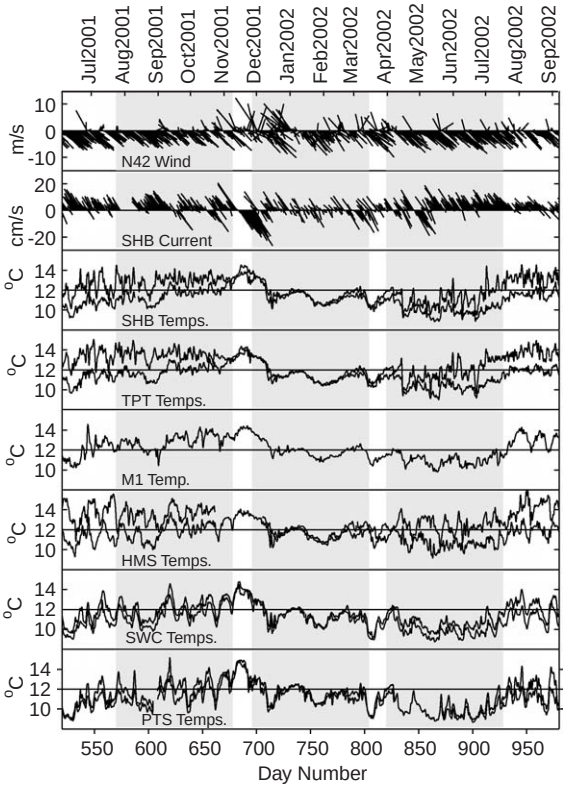

Fig. 2. Monterey Bay area low-frequency winds, currents, and bottom and top water temperatures, June 2001–September 2002. Shaded areas denote distinct oceanographic seasons: spring upwelling, fall relaxation, and winter storm. For the stick plots, northward is toward the top of the page, and a vectors' magnitude can be scaled on the *y*-axis. SHB current is a depth-average. Monthly tick marks (top *x*-axis) fall on the first of the month.

polarization, ellipticity ~2. Relative to spring and fall, winds and currents were less polarized in the winter, typically by a factor of 2–3 for winds and 1.5–2 for currents. The directions of the major axes also varied slightly from season to season ($\Delta\theta < 10^{\circ}$), with the biggest differences found with respect to the winter orientations. However, the results presented in this study were not sensitive to such small changes in axes orientation.

All temperature measurements (Fig. 2) showed seasonal behavior consistent with previous observations made within Monterey Bay (Graham and Largier, 1997) and over the central and northern California shelf (Largier et al., 1993; Lentz, 1987; Strub et al., 1987). Monthly means of bottom and

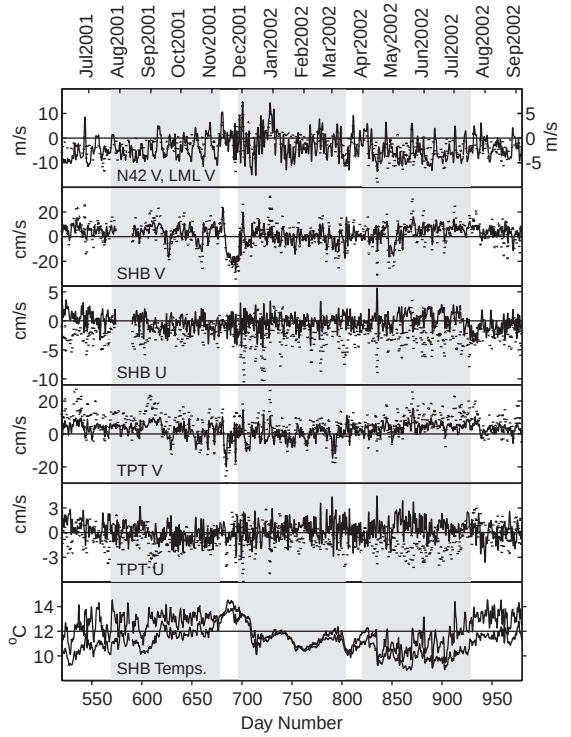

Fig. 3. Low-frequency winds and currents from northern Monterey Bay. Shaded areas denote oceanographic seasons defined in text. LML winds (dotted) are scaled on the right-hand axis. v is alongshore velocity component, u the cross-shore. At (SHB, TPT) dotted lines represent near-surface (2, 3 m depth) currents, and solid lines represent near-bottom (17, 15 m depth) currents. Monthly tick marks (top x-axis) fall on the first of the month. Top and bottom SHB temperatures are also shown for comparison of annual temperature cycle (see Fig. 2).

top temperatures displayed a minimum in spring (April in 2001 and May or June in 2002), a month or two after the wind turned steadily southeastward. During both 2001 and 2002, bottom and top temperatures then steadily rose throughout the remaining spring and summer, with monthly mean bottom temperatures reaching a maximum in November. Monthly mean top temperatures either peaked in November with bottom temperatures, or reached a maximum earlier in summer (September for TPT in 2001 and August for HMS in 2002). Temperatures declined during the winter storm season (December to February), when the water column was well-mixed.

Table 4

	Fall 2001		Winter 2001–2002		Spring 2002	
	Mean	Std	Mean	Std	Mean	Std
(a) Basic seasonal current and wind statistics[a]						
Wind or current station						
LML v (m/s)	−1.3	1.0	−0.1	1.8	−2.7	1.8
LML u (m/s)	0.4	0.5	−0.2	1.8	0.5	0.8
N42 v (m/s)	−4.1	3.7	−2.2	5.6	−5.6	4.2
N42 u (m/s)	0.5	0.6	0.0	2.1	1.0	0.8
SHB v (cm/s)	4.8	7.1	−0.3	7.3	4.8	7.7
SHB u (cm/s)	−0.2	0.7	−0.6	1.1	−0.3	0.7
TPT v (cm/s)	5.4	5.7	0.4	5.7	6.7	4.2
TPT u (cm/s)	0.4	0.7	0.2	0.8	0.4	0.6
(b) Basic seasonal temperature statistics[b]						
Temperature station						
SHB top	13.0	0.6	11.6	0.7	11.2	0.9
SHB bottom	11.6	0.5	11.4	0.6	10.0	0.6
TPT top	13.5	0.5	11.6	0.7	11.8	0.8
TPT bottom	12.0	0.5	11.4	0.6	10.4	0.6
M1 10 m	12.8	0.6	11.9	0.6	11.0	0.5
HMS top	13.6	0.7	12.1	0.8	12.5	0.7
HMS bottom	11.9	0.7	11.6	0.7	10.7	0.6
SWC top	12.2	0.8	11.5	0.7	10.7	0.7
SWC bottom	11.5	0.8	11.2	0.7	9.9	0.7
PTS top	12.2	0.9	11.7	0.7	10.2	0.9
PTS bottom	11.4	0.8	11.4	0.7	9.7	0.8

[a]Currents statistics refer to depth-averages. See Tables 2 and 3 for axis definitions.
[b]All temperature statistics in °C.

Mean temperatures were highest at HMS and TPT, sites in and near Monterey Bay's southern and northern bights, respectively (Table 4b). During spring and fall, SHB temperatures were consistently below TPT temperatures at all measured depths. SWC and PTS, south of the bay, were consistently the coolest sites. The relatively warm temperatures at TPT were consistent with the persistent warm temperature zone, or "upwelling shadow," previously observed in Monterey Bay's northern bight (Graham and Largier, 1997). The temperature stratification at most sites peaked in mid-summer (June and July in 2001, and July and August in 2002). Stratification was highest at HMS, with typical top-sensor-to-bottom-sensor, mid-summer, daily values of ~0.25–0.35 °C/m. Values were slightly less at TPT and SHB, but substantially less (~0.05–0.1 °C/m) south of Monterey Bay at SWC and PTS. These peak summer-

time stratification values are about two or three times the fall (108-day) averages. These vertical temperature gradients are consistent with prior inner shelf measurements from within Monterey Bay (~0.2 °C/m, Graham and Largier, 1997). But note that the stratification reported here is relatively large compared to other reported summertime measurements at similar depths on the northern California inner shelf (~0.02 °C/m, Lentz, 1994), and deeper nearby shelf measurements (~0.01 °C/m, Ramp and Abbott, 1998). The measurements reported here are closer to those reported for the Southern California Bight (Pringle and Riser, 2003). The relatively large stratification values indicate that vertical mixing may have been reduced in the water column's interior, despite the shallow overall water depth. Bulk gradient Richardson number (Ri) calculations, based on hourly, unfiltered thermistor and ADCP data at SHB and TPT show much scatter, but give $Ri \geqslant 0.25$. These calculations, though imprecise due to the separation of the sensors, suggest a near-inviscid interior existed with relatively thin (~1–5 m) top and bottom boundary layers.

Throughout the spring, summer and early fall, the temperature record at all inner shelf sites was punctuated by ~0.5–3 °C increases in temperature lasting 2–20 days. These temperature fluctuations were observed throughout the water column and are shown in Section 3.4 to be caused by relaxations of the predominantly southeastward wind stress. With the exception of at SWC, these relaxation events also noticeably strengthened the temperature stratification, with top sensors experiencing more warming. At SWC, the fluctuations were of approximately equal magnitude throughout the water column.

The current records displayed high variability year-round, with standard deviations of both alongshore (v) and cross-shore (u) depth-averaged velocities usually larger than their respective seasonal means (Table 4a). But a relatively consistent, northwestward (poleward) mean flow was observed at both SHB and TPT during spring and fall (Fig. 3). This northwestward flow relaxed to a near-zero mean during winter. The northwestward flow is consistent with existing measurements in northern Monterey Bay. Prior long-term current observations at SHB and near TPT display northwestward means (Breaker and Broenkow, 1994; Storlazzi et al., 2003). High-frequency radar measurements show cyclonic, basin-scale surface flow inside the bay, northwestward near TPT, in late summer and fall (Paduan and Rosenfeld, 1996). And a smaller-scale, cyclonic flow pattern in the bay's northern bight has been inferred based on the hydrgography of the upwelling shadow (Graham and Largier, 1997), implying northwestward near-surface flow near TPT.

At SHB, monthly means of depth-averaged alongshore flow displayed maximums in May of 2001 and July of 2002 (monthly averages not shown). At TPT, the maximums were in August of 2001 and June of 2002. (Compare with N42's June maximums in southeastward wind velocity.) The annual signal in alongshore currents was approximately π radians out of phase with the annual wind signals at N42 and LML, with a seasonal mean northwestward current flowing in direct opposition to a southeastward wind stress during spring and fall (Fig. 3 and Table 4a). It is common for mean currents on the central and northern California shelf to flow northward in opposition to southward or southeastward winds (Chelton et al., 1988; Largier et al., 1993; Lentz, 1994; Ramp and Abbott, 1998; Strub et al., 1987), especially during late summer and winter. But this northward flow is usually preceded by a period of southward flow during the spring, at least at the surface. Previous authors have invoked a northward-forcing (i.e. negative) alongshore pressure gradient to explain these seasonal periods of northward flow during times of southward wind stress (Largier et al., 1993; Lentz and Trowbridge, 2001).

3.2. Seasonal scaling

The unusual wind-current phasing and other seasonal dynamics in northern Monterey Bay were investigated by scaling the various terms in the momentum equations, with calculations made directly from the data when possible. An alongshore pressure gradient was found to be of primary importance here as well. Using the following notation to define the linear and non-linear

transports,

$$M^{(u,v)} = \int_{-H}^{\eta} (u, v)\, dz,$$

$$M^{(uu,vv)} = \int_{-H}^{\eta} (uu, vv)\, dz,$$

$$M^{uv} = \int_{-H}^{\eta} uv\, dz,$$

the depth-integrated alongshore momentum equation can be written:

$$M^v_t + M^{uv}_x + M^{vv}_y + fM^u = -\frac{gH^2}{2\rho_0}\rho_y - g(H+\eta)\eta_y + \rho_0^{-1}\tau^y_w - \rho_0^{-1}\tau^y_b. \quad (1)$$

Here, u and v are the cross- and alongshore components of velocity, ρ is the perturbation density, ρ_0 is a reference density, η is the sea surface height, $\tau^y_{(w,b)}$ are the wind and bottom stresses, H is the water depth, and subscripts refer to differentiation. The pressure has been linearized about $z = 0$, the still sea surface. Horizontal density gradients were assumed to be depth-independent. With the same assumptions and notation, the depth-integrated cross-shore momentum equation becomes

$$M^u_t + M^{uu}_x + M^{uv}_y - fM^v = -\frac{gH^2}{2\rho_0}\rho_x - g(H+\eta)\eta_x + \rho_0^{-1}\tau^x_w - \rho_0^{-1}\tau^x_b. \quad (2)$$

The seasonal averages of the measured terms are given in Table 5. The values are representative of seasonal and perhaps monthly timescales, $T \sim 30$–108 days. Wind stresses were calculated using the method of Large and Pond (1981) using data from LML. Bottom stresses were estimated using the velocity in the lowest ADCP bin, a quadratic drag law, and a drag coefficient of 5×10^{-3} (Lentz, 1994). Velocities used to estimate the transports and bottom stresses were first rotated into a common reference frame with alongshore (y) axis oriented along a line joining TPT and SHB, positive toward SHB. Transports and stresses were then either averaged or differenced between the two sites, centering the estimates. This increased their accuracy, but precluded the calculation of cross-shore gradients. The portions of the water column unresolved by the ADCP were ignored in the transport calculations. The baroclinic pressure gradient, the first term on the right-hand-side of Eq. (1), was estimated using the equation of state of seawater, the average temperature difference between the three sensors on each mooring, an assumed salinity of 33.5 PSU (Breaker and Broenkow, 1994), and zero pressure.

No obvious, simple balance is apparent in the alongshore momentum equation during winter, but during fall and spring a dominant balance involving the wind stress and pressure gradients can be inferred. There is no measured term with

Table 5
Dynamic scaling

Alongshore depth-integrated momentum equation

	M^v_t	M^{uv}_x	M^{vv}_y	fM^u	$-1/2gH^2\rho_0^{-1}\rho_y$	$-g(H+\eta)\eta_y$	$\rho_0^{-1}\tau^y_w$	$-\rho_0^{-1}\tau^y_b$
Fall	-7×10^{-8}	—	5×10^{-6}	1×10^{-6}	-2×10^{-5}	—	-1×10^{-5}	-6×10^{-6}
Winter	3×10^{-7}	—	6×10^{-6}	-5×10^{-6}	-2×10^{-6}	—	-2×10^{-6}	2×10^{-6}
Spring	2×10^{-7}	—	7×10^{-6}	-2×10^{-6}	-2×10^{-5}	—	-3×10^{-5}	-9×10^{-6}

Cross-shore depth-integrated momentum equation

	M^u_t	M^{uu}_x	M^{uv}_y	$-fM^v$	$-1/2gH^2\rho_0^{-1}\rho_x$	$-g(H+\eta)\eta_x$	$\rho_0^{-1}\tau^x_w$	$-\rho_0^{-1}\tau^x_b$
Fall	-2×10^{-8}	—	9×10^{-6}	-8×10^{-5}	—	—	4×10^{-6}	9×10^{-7}
Winter	4×10^{-8}	—	6×10^{-6}	-2×10^{-6}	—	—	4×10^{-6}	5×10^{-7}
Spring	3×10^{-8}	—	1×10^{-5}	-9×10^{-5}	—	—	8×10^{-6}	-4×10^{-7}

Values are seasonal means. Units are m^2/s^2.

the proper sign and size to balance the combination of the wind stress and baroclinic pressure gradient on the right-hand side of Eq. (1) (Table 5). The magnitude of the wind stress is likely an underestimate, as it was based on data from a land station (Halliwell and Allen, 1987). The cross-shore advection term M_x^{uv} was not measured directly, but it can be easily scaled. Using a cross-shore length scale for the alongshore current of 10 km, given the observed bottom slope, and assuming currents will approximately follow isobaths, M_x^{uv} will scale like $\sim 1 \times 10^{-6}\,\mathrm{m^2/s^2}$. This leaves only the unmeasured barotropic pressure gradient available to balance the wind stress and baroclinic pressure gradient in Eq. (1). Such a pressure gradient corresponds to a sea-surface slope of 5×10^{-7}, with the sea surface higher to the southeast, inside the bay.

Turing to the cross-shore momentum Eq. (2), the dominant balance appears to be geostrophic in fall and spring, as traditionally assumed, but not so in winter. In fall and spring, the Coriolis acceleration is by far the largest measured term. It can only be balanced by one of the pressure terms or the cross-shore advective term M_x^{uu}. This term was also not directly measured, but scaling it with the same assumptions as M_x^{uv} yields a value of $\sim 1 \times 10^{-6}\,\mathrm{m^2/s^2}$, much too small to balance the Coriolis acceleration. Previous hydrographic measurements near TPT suggest that the cross-shore baroclinic pressure gradient is positive ($\rho_x < 0$), with warmer water closer to shore (Graham and Largier, 1997). If this is the case, only the barotropic cross-shore pressure gradient can balance the Coriolis term in fall and spring. This implies positive sea surface setup at the coast, despite the mean southeastward winds observed at LML and N42 and their implied offshore Ekman transport. In winter, the Coriolis acceleration is not a dominant term due to the near-zero mean alongshore current, and there is apparently no simple geostrophic balance, at least not on the seasonal timescale.

3.3. Mean velocity profiles

Seasonal mean velocity profiles (Fig. 4) were similar at SHB and TPT. But alongshore spring profiles at both sites differed substantially from previous observations made on the California coast (Winant et al., 1987; Largier et al., 1993) and at other upwelling regions (Smith, 1981). As noted in Section 3.1, alongshore mid-shelf currents in upwelling regions during spring and early summer are typically equatorward near the surface, although poleward subsurface flow may be present. Spring profiles observed here were northwestward (poleward) at all depths. However, fall alongshore profiles at SHB and TPT were similar to earlier fall shelf observations made in northern California (Lentz and Trowbridge, 2001), displaying northwestward flow at all depths and a mid-depth maximum. During all seasons, the vertical shear in the alongshore current was slightly larger at TPT relative to SHB. The winter displayed surprisingly small alongshore means at all depths with relatively little shear, especially at SHB.

Cross-shore profiles were comparatively invariant between seasons and were consistent with previous shelf observations from regions with poleward subsurface shelf flow (Smith, 1981). Cross-shore profiles are also consistent with a two-dimensional conceptualization of upwelling, where offshore Ekman transport at the surface, caused by a mean equatorward (southeastward) wind, is balanced by a compensatory onshore flow

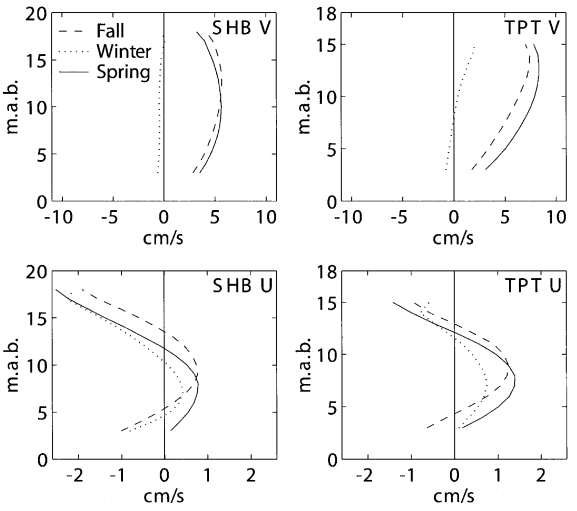

Fig. 4. Seasonal means of alongshore (v) and cross-shore (u) velocities. Top of panel represents Mean Lower Low Water (MLLW).

at depth. This onshore flow was strongest at mid-depth and was in approximate geostrophic balance with the previously deduced alongshore pressure gradient (Table 5). The onshore flow weakened near bottom and even turned negative (offshore) in some instances. Smith (1981) suggested that frictional veering of the poleward interior flow may be responsible for this near-bottom weakening in the onshore velocity. But this weakening was also present at SHB and TPT during winter, when the alongshore near-bottom velocity was southeastward (equatorward) or negligible. The dynamics of the cross-shore flow in this portion of the water column on the California shelf appears to be complex and cannot in general be explained by a balance between the Coriolis force and bottom stress (i.e. frictional veering, Lentz and Trowbridge, 2001).

3.4. Remote wind forcing

Although generally important on the northern California shelf, remote wind forcing was found to be of secondary, if any, importance to both temperatures and currents at PISCO inner shelf sites. Researchers have used wind correlations from sites "upstream" in the coastally trapped wave sense, in this case southward, to explore the importance of remote forcing on currents and temperatures. Remote winds approximately 175–500 km south of research sites were found to be important along the California coast (Davis and Bogden, 1989; Denbo and Allen, 1987; Largier et al., 1993; Pringle and Riser, 2003).

The springtime maximum lagged correlations of alongshore winds vs. SHB and PTS top temperatures are given in Table 6 for each wind station listed in Table 2. Correlations and lags were positive and relatively constant from N12 at Half Moon Bay south to N11 near the mouth of the Santa Maria River. LML was the exception and showed a relatively low correlation with PTS top temperature (explored in detail below). South of Point Conception (the large promontory on the California coast near the "Y" in Fig. 1) at N53 and N25, the correlations decreased substantially, and in the case of PTS, became insignificant. This suggests little or no remote forcing from below Point Conception and a relatively constant wind field between Point Conception and the Monterey Bay area. Bottom temperatures also showed no signs of remote forcing. Wind-current correlations displayed a different pattern (Table 6). Springtime correlations of alongshore winds with the depth-averaged alongshore current at SHB were highest at LML and AQ, the two land stations closest to SHB, and were relatively constant elsewhere when significant. This also argues against any remote wind influence. (The negative correlations at large lags (~10 days) at SUR and N28 are most likely spurious and were not significant to the 99% confidence limit.) Although correlations were generally less during fall and winter, spatial patterns during these seasons were similar to spring: PTS top temperature showed relatively constant wind correlations north of N11, decreasing substantially south of Point Conception. And SHB wind-current correlations were highest at LML. SHB top temperature correlations were not significant in winter, but showed a pattern similar to spring in fall. These positive correlations and lags indicate that temperatures and alongshore currents follow the wind, with wind relaxations

Table 6
Spring remote forcing correlations

Wind station	Observable					
	SHB top temp.		PTS top temp.		SHB v	
	r	Lag (days)	r	Lag (days)	r	Lag (days)
N12	0.63	0.63	0.71	0.96	0.32	0.29
LML	0.66	0.75	0.43	1.29	0.53	0.29
N42	0.62	0.54	0.76	0.92	0.29	0.21
M1	0.65	0.58	0.73	0.96	0.34	0.21
AQ	0.66	0.63	0.64	1.08	0.44	0.21
SUR	0.60	0.58	0.78	1.00	(−0.29)	9.50
N28	0.64	0.58	0.80	1.04	(−0.27)	9.63
N11	0.62	0.88	0.74	1.29	0.35	0.13
N53	0.49	1.33	(0.35)	2.08	0.39	0.21
N25	0.35	1.71	(0.24)	−9.63	0.29	0.83

v refers to depth-averaged alongshore current. Positive lag indicates that the time series follows the wind. Wind–temperature correlations in parenthesis were not significant to the 95 percent confidence level. Parentheses indicate the 99 percent limit for wind–current correlations.

Table 7
Spring wind–wind correlations

Wind station	Wind station											
	LML		N42		M1		AQ		SUR		N28	
	r	Lag	*r*	Lag	*r*	Lag	*r*	Lag	*r*	Lag	*r*	Lag
N12	0.54	0.04	0.96	−0.04	0.91	−0.04	0.86	0.00	0.82	0.04	0.87	0.04
LML	1.00	0.00	0.49	−0.08	0.57	0.00	0.66	−0.04	0.42	−0.17	0.46	−0.17
N42	0.49	0.08	1.00	0.00	0.93	0.00	0.85	0.04	0.90	0.04	0.93	0.04
M1	0.57	0.00	0.93	0.00	1.00	0.00	0.91	0.00	0.89	0.04	0.91	0.00
AQ	0.66	0.04	0.85	−0.04	0.91	0.00	1.00	0.00	0.76	−0.04	0.82	−0.04
SUR	0.42	0.17	0.90	−0.04	0.89	−0.04	0.76	0.04	1.00	0.00	0.96	−0.04
N28	0.46	0.17	0.93	−0.04	0.91	0.00	0.82	0.04	0.96	0.04	1.00	0.00
N11	0.55	0.25	0.76	−0.25	0.77	−0.04	0.76	0.04	0.84	−0.13	0.87	−0.13
N53	0.56	0.21	(0.27)	4.67	0.33	4.42	0.38	−0.04	0.28	4.75	0.27	−0.96
N25	0.32	0.04	(−0.27)	1.04	0.29	4.25	0.29	10.8	−0.35	0.83	−0.31	1.33

Positive lags indicate the wind station in the column header leads. Lags are in days. Correlations in parenthesis were not significant to the 99 percent confidence level.

resulting in warming at PTS and both warming and northwestward velocity fluctuations at SHB.

High wind vs. wind correlations at short lags (Table 7) indicate a spatially coherent wind field existed along California's coast between Half Moon Bay and Point Conception during spring. Most Monterey Bay area stations, LML, N42, M1, AQ, SUR, were well correlated ($r \sim 0.8$–0.9) with all stations north of Point Conception at lags of a few hours. LML was an exception, displaying relatively low ($r \sim 0.5$–0.6), although significant, correlations with its neighboring stations. This difference in wind–wind correlation strength relative to LML ($r \approx 0.9$ vs. $r \approx 0.5$) was itself significant to the 99% confidence level. Fall and winter showed a pattern similar to that in spring: wind–wind correlations were high north of Point Conception, except vs. LML, where they were relatively low. These results are generally consistent with the findings of Halliwell and Allen (1987), who showed that most of the wind variance along the US west coast was due to fluctuations with alongshore wavelengths >900 km. With the exception of LML, note the sharp drop in correlation values of Monterey Bay area stations with stations below Point Conception (N53 and N25), approximately 400–500 km to the south (Table 2). This distance is roughly consistent with the ~450 km spatial integral correlation scale calculated for alongshore winds by Halliwell and Allen (1987). LML's anomalously low correlations with its neighbors suggest that the site has a comparatively short spatial integral correlation scale and that most of the station's variance cannot be attributed to large-scale, regional (>500 km) wind fluctuations.

3.5. *Temperature variability and its associated wind forcing*

The variance-preserving spectra of top and bottom temperatures at TPT and SWC are shown in Fig 5; the TPT temperature spectra are generally representative and sites inside or to the north of the bay (SHB, TPT, HMS), and the SWC spectra are generally representative of sites south of the bay (SWC, PTS). Temperature spectra were of two main shapes: one shape displayed a single, broad peak at long periods (20–50 days) and was typical of the winter spectra at all sites. The second shape was double-peaked with power concentrated at both long periods (20–50 days) and short to mid-periods (3–15 days). This shape was typical of fall and spring (e.g. TPT bottom, spring). The double peaks often merged together with averaging, creating a broad, single peak at long to mid-periods during fall and spring (e.g. SWC top, fall). Note the frequency resolution on these plots at

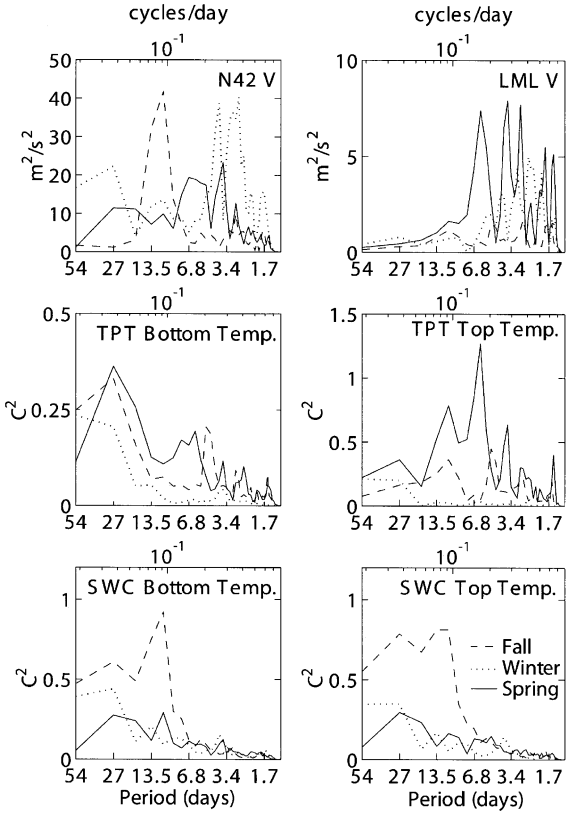

Fig. 5. Variance-preserving power spectra of N42 and LML alongshore winds and TPT and SWC temperatures for all three seasons.

long periods, $T>20$ days, where T is the period, was rather poor. Except for top temperatures at SHB, TPT and HMS, the temperature variance was concentrated at periods longer than 10 days. The concentration of spectral power at low frequencies was especially pronounced during winter at the northern sites SHB, TPT and M1 (SHB and M1 not shown), where there was almost no variance at periods shorter than 10 days. This feature can be readily seen in the time domain (Fig. 2). Spring bottom and top spectra at TPT and SHB displayed a distinct peak between 3 and 12 days. This peak is largest in the top temperature spectra, where it dominates the overall temperature variance. Top temperatures at SHB and TPT, the two northernmost sites, showed the largest high-frequency variance.

Wind spectra at N42 (Fig. 5) displayed a large variation in the frequency distribution of variance between seasons and were generally dissimilar from the temperature spectra. For N42, a well-defined, relatively narrow peak near 12 days dominates the fall spectra; a broad band of power between 3 and 25 days defines the spring spectra, and the winter is characterized by two major loci of power, one near 3–5 days and another around 25–50 days. LML's wind spectra (Fig. 5) showed comparatively less power at long periods, with most of the winter and spring variance concentrated at periods shorter than a week. Fall spectra at LML did share N42's peak near 12 days, but the feature was much less pronounced.

The coherence of temperature between sites can reveal the spatial scale of the fluctuations described by the power spectra. Coherence plots of SHB bottom and top temperatures vs. the respective bottom and top temperatures of the other inner shelf sites, as well as M1's 10 m temperature, are shown in Fig. 6. The calculation was made over the complete year given in Table 3. The coherence function, γ^2, is analogous to r^2, the square of the correlation coefficient, and can be thought of as how well two variables are correlated over a given frequency band (Bendat and Piersol, 2000, Chapter 6). The longest periods, $T>15$ days, showed the highest coherence, with little or no statistically significant coherence at shorter periods. TPT, located less than 10 km from SHB, was the exception and showed significant coherence with both SHB bottom and top temperatures from periods of 2–60 days. At all sites, when the coherence was significant, the phase was not statistically different from zero, indicating temperatures essentially fluctuate in-phase at long periods ($T>15$ days) along the inner shelf in the Monterey Bay area.

The importance of local wind forcing to the temperature field in the area can be seen in Fig. 7, which shows the coherence of alongshore winds vs. inner shelf bottom temperatures and M1's 10 m temperature. As with the temperature-vs.-temperature coherence, the highest coherence was found at the longest measured periods (15–60 days). These periods correspond loosely to the periods of the highest temperature power (Fig. 5). When calcu-

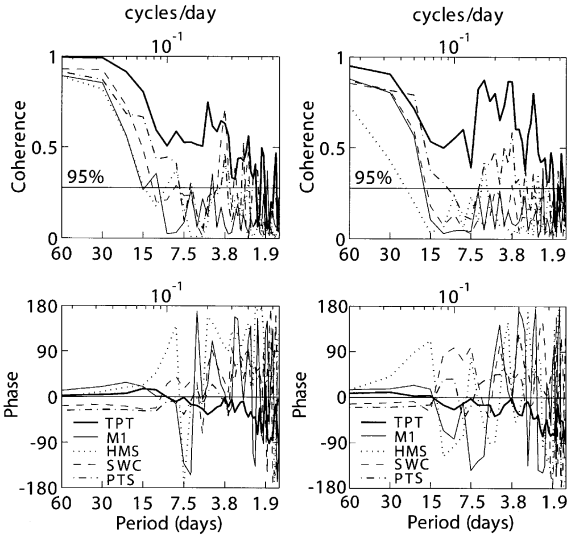

Fig. 6. Alongshore temperature vs. temperature coherence. Coherence and phase of SHB bottom temperature (left panels) and top temperature (right panels) vs. all bottom temperatures (left) and all top temperatures (right). M1 10 m temperature included in both left and right panels. Coherence calculation was made over complete year given in Table 3. Horizontal line is the value where coherence becomes statistically significant from zero to the 95% confidence level. Positive phase indicates that temperature signal follows SHB.

lated over a complete year as shown in Fig. 7, there was little or no difference between the coherence calculated using winds at N42 and winds from a station substantially closer to each individual temperature mooring. Note SWC and PTS generally displayed the highest wind coherence, and only PTS showed consistently significant coherence at all measured frequencies. At all sites the phase was positive and, at most frequencies, also significant when the coherence was significant, indicating that a positive temperature fluctuation follows a positive wind fluctuation. This is consistent with a basic two-dimensional understanding of upwelling along California's coast, where a wind relaxation (i.e. a positive, northward wind fluctuation) results in warming near the shore. The influence of the wind can also be easily seen in the time domain (Fig. 8), where temperatures appear to track the wind.

The temperature response to wind forcing, as evidenced by the maximum lagged cross-correlation of the two variables, showed distinct differences both between seasons and sites. Maximum lagged correlations were highest during fall and spring (Tables 8a and b), and highest at the two southernmost sites outside Monterey Bay, SWC and PTS. These sites also had the coldest means during spring and fall. Except for TPT top temperature, wind–temperature correlations did not improve relative to N42 by using winds from a station closer to a given temperature mooring. The negative correlations found during winter at large lags ($\pm$6–10 days) for stations SHB, TPT, M1 and HMS were not statistically significant and were the result of the proportionately high long-period variance in the temperature records at these sites. These records were almost sinusoidal with a period of ~40–60 days, resulting in few effective degrees of freedom and relatively high, periodic correlations at large lags, both positive and negative. Bottom and top temperatures at the two northernmost sites (SHB and TPT), as well as M1's 10 m temperature, were most correlated with winds during spring. Wind correlations were slightly higher for top temperatures than for bottom temperatures at SHB and TPT during this season, and correlations were highest vs. LML winds. HMS temperatures, however, both top and bottom, showed the strongest wind response during fall. At this site wind correlations were highest with the bottom rather than the top temperature. Compared to the other sites, SWC and PTS wind–temperature correlations were relatively high during all three seasons, with the lowest—but still significant—values found in winter. These fall/spring and top/bottom differences in correlations were, in most cases, not significant to the 95% confidence level.

Note the relatively long lags displayed by the HMS top temperature with respect to winds during fall and spring. This sensor can be seen to be noticeably out of phase with the bottom sensor during fall (Fig. 2), an apparent feature of mixed layer dynamics. In general, HMS showed the least intra-mooring bottom-vs.-top temperature coherence of all the inner shelf sites. SWC and PTS showed the tightest intra-mooring relation between bottom and top temperatures, with significant coherence extending from periods of 3–60

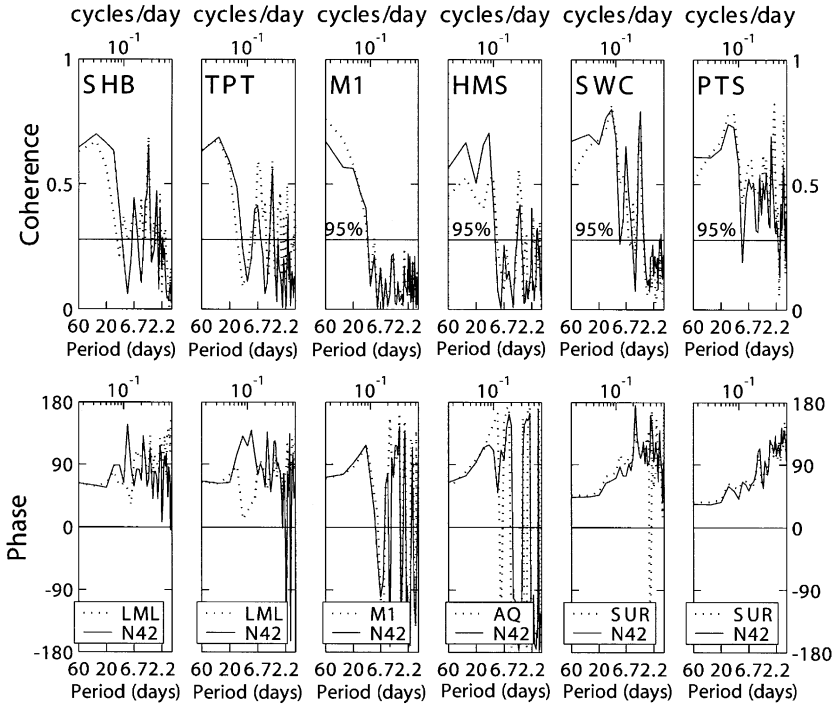

Fig. 7. Wind vs. temperature coherence for bottom temperatures at all inner shelf moorings and M1 10 m depth. Horizontal line is the value where coherence becomes statistically different from zero. At most sites and frequencies with significant coherence, the phase was positive and significant, indicating that temperatures lag the wind.

days (not shown), and almost complete coherence ($\gamma^2 \sim 0.95$) between 10 and 60 days. At most sites, where bottom-vs.-top temperature coherence was significant, the phase was not significantly different from zero, indicating that the bottom and top temperatures fluctuate in-phase. HMS was the exception, with top temperatures lagging bottom temperatures at long periods and a confused phase relationship at short periods. The near-zero phase relationship between bottom and top temperatures at most sites argues that the correlations of winds and top temperatures (Table 8b) are not artifacts of wind-induced near-surface mixing, but are predominantly the result of advection (vertical and/or horizontal) of cold, upwelled water throughout the water column.

Although something of an anomalous wind station, LML strongly influenced temperatures and currents (Section 3.6) in its immediate area. This influence on temperature can best be seen by examining the coherence of winds vs. top temperatures during spring (Fig. 9). Note the high coherence of SHB and TPT temperatures with LML's wind signal relative to N42's. The difference was significant at both sites, but the feature was limited to the spring season. This contrasts with Fig. 7, the same calculation made over a full year, where there was little difference in response to the two wind signals. The averaging over seasons inherent in the annual calculation masked the feature. Springtime bottom temperatures at SHB and TPT displayed the same pattern (high coherence vs. LML, low vs. N42) at periods of 2–9 days, and were not significantly coherent with either wind station at 18 days. In general, seasonal patterns in wind–temperature coherence were similar to the patterns in the wind–temperature correlations discussed above: coherences were highest with SWC and PTS during fall and spring, with the exception of the high springtime coherences found with LML winds at SHB and TPT.

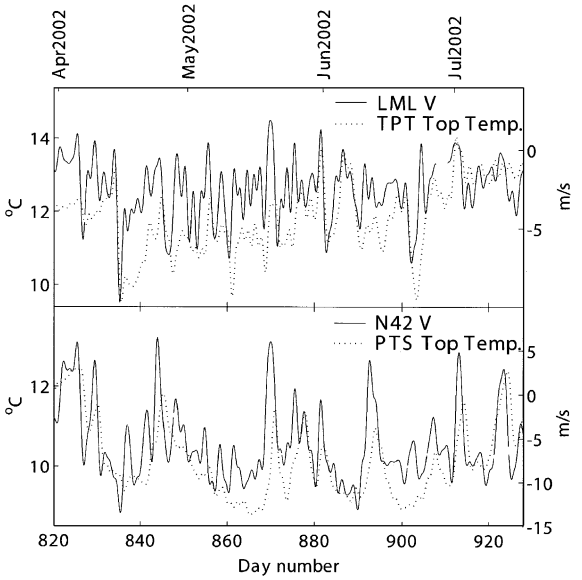

Fig. 8. Time history plot of TPT top temperature and LML alongshore wind (top panel) during spring, showing strong positive correlation, $r = 0.68$, between winds and temperature. Maximum correlation was found when TPT top lagged LML wind by 14 hours. Bottom panel shows that PTS top temperature is well-correlated with N42 winds, $r = 0.76$, with temperatures lagging winds by 22 h. Monthly tick marks fall on the first of the month.

3.6. *Velocity fluctuations and their associated wind forcing*

Current velocities also displayed a strong response to the wind, especially during spring, although there were substantial differences with the wind/temperature behavior. Near-surface velocity spectra (Fig. 10) showed proportionately much less low-frequency power than temperature spectra. Alongshore velocity spectra at both SHB and TPT were roughly similar to N42's spectra during spring, displaying one broad band of power between 3 and 25 days. Relative to alongshore velocities, cross-shore velocities showed proportionately more variance at higher frequencies: Note the fairly well-defined peak in SHB cross-shore power near 3.5 days during winter and spring. Near-bottom velocities showed similar spectra (not shown) to near-surface currents, although the absolute power was much reduced in the alongshore component.

It was found that the velocity fluctuations were best described with an empirical orthogonal decomposition (Kundu et al., 1975), as just two empirical orthogonal functions, or EOFs, could describe most of the variance in either velocity component. The EOF decomposition is a statistical treatment requiring no dynamical assumptions. It reduces the data into spatial (in this case, vertical) modes, each with its own time-dependent amplitude. The data can be reproduced as a linear combination of the modes, each mode modulated by its respective time-dependent amplitude. This treatment also has the advantages that the modes are orthogonal in space, uncorrelated in time, and each mode's contribution to the overall variance is readily calculated. In the decomposition, the velocity components were treated separately as scalars.

The largest two mode shapes at SHB and TPT for both the alongshore (v) and cross-shore (u) velocity for each season are shown in Figs. 11 and 12. The percent variance explained, or overall contribution of each mode to the variance of its respective velocity component, is also given in Table 9. The first alongshore mode (SHB v 1st, TPT v 1st) represented vast bulk (84–97%) of the alongshore variance at both sites. As the alongshore variance dwarfs the cross-shore variance (Fig. 10), these modes also represented the bulk of the total current variance ($[\sum \mathrm{var}(u) \sum + \mathrm{var}(v)]$, where the sum is over the water depth). At both sites, the two largest alongshore modes were remarkably invariant between seasons. The relatively noisy shape of the alongshore second mode at SHB during fall can be attributed to the white noise used to fill a 16-day gap in August of 2001 (Fig. 2). The alongshore first mode lacked a zero-crossing at both sites and was similar to the mean alongshore velocity profiles found during fall and spring (Fig. 4). This was particularly true at TPT, indicating that the shape of the mean alongshore velocity profile was also representative of the fluctuations during these seasons. In another similarity to the mean profiles, the alongshore first mode at TPT displayed slightly more shear relative to SHB during fall and spring.

Unlike the alongshore modes, the cross-shore second modes each represented a sizable fraction

Table 8

Station pairing	Season					
	Fall		Winter		Spring	
	r	Lag (days)	*r*	Lag (days)	*r*	Lag (days)
(a) *Wind-bottom temperature correlations*[a]						
N42 vs. SHB	(0.37)	3.33	(−0.46)	−9.79	0.53	1.13
LML vs. SHB	(−0.31)	−10.6	(−0.41)	−9.79	0.46	0.71
N42 vs. TPT	0.45	5.50	(−0.44)	−9.92	0.53	4.13
LML vs. TPT	0.41	9.00	(−0.40)	−9.88	0.47	0.54
N42 vs. M1	(0.34)	6.00	(−0.31)	−5.58	0.48	3.42
M1 vs. M1	(0.37)	4.67	(−0.34)	−5.63	0.48	3.46
N42 vs. HMS	0.55	3.67	(0.41)	8.50	0.50	2.83
AQ vs. HMS	0.57	3.42	(−0.36)	−6.46	0.51	5.75
N42 vs. SWC	0.67	2.29	0.51	1.33	0.73	1.13
SUR vs. SWC	0.72	2.13	0.45	1.46	0.68	1.50
N42 vs. PTS	0.62	1.04	0.58	0.96	0.76	0.79
SUR vs. PTS	0.70	1.00	0.55	0.88	0.76	0.88
(b) *Wind-top temperature correlations*[a]						
N42 vs. SHB	0.40	0.29	(−0.36)	−9.50	0.62	0.54
LML vs. SHB	0.46	0.71	(−0.36)	−5.38	0.66	0.75
N42 vs. TPT	0.33	8.54	(−0.36)	−8.00	0.34	4.96
LML vs. TPT	0.49	0.46	(−0.39)	−5.29	0.68	0.58
N42 vs. HMS	0.47	6.33	(−0.34)	−10.5	0.34	8.21
AQ vs. HMS	0.44	6.13	(−0.40)	−10.8	0.35	8.13
N42 vs. SWC	0.63	2.79	0.45	6.00	0.63	0.92
SUR vs. SWC	0.67	2.75	(0.42)	6.13	0.59	1.25
N42 vs. PTS	0.62	1.17	0.48	1.13	0.76	0.92
SUR vs. PTS	0.73	1.08	0.48	1.04	0.78	1.00

[a]Positive lag that indicates that wind leads temperature. Correlations in parenthesis were not significant to the 95 percent confidence level.

of the variance at both sites. However, the first mode (SHB *u* 1st, TPT *u* 1st) usually accounted for at least 50% of the variance (the exception being SHB fall). Cross-shore mode shapes were approximately invariant between seasons at SHB, but mode shapes showed distinct seasonal variations at TPT. Despite the differences between seasons at this site, there were only two basic shapes observed. One shape displayed near-surface and near-bottom extrema and a mid-depth zero-crossing (spring first mode, fall and winter second mode), and the other shape displayed a mid-depth extremum and no zero-crossing (spring second mode, fall and winter first mode). The first cross-shore mode shapes were generally different from the mean cross-shore velocity profiles, indicating that the mean profile was not representative of a typical fluctuation for this component.

Similar to temperatures, currents also displayed distinct wind responses between seasons and sites. Alongshore first modal amplitudes showed the highest wind coherence during the spring upwelling season (Fig. 13). Coherences of LML winds vs. SHB *v* 1st were also significant during the fall and winter, although to a much reduced extent (Fig. 14, fall not shown). TPT first modal amplitudes, both along- and cross-shore (*u*, *v* 1st), did not display consistently significant coherence with winds during fall and winter. Similar to top temperatures, springtime alongshore modal amplitudes at SHB and TPT showed substantially higher coherence vs. the LML wind signal relative to N42. The difference was significant to the 95% confidence level. This demonstrates the importance of these local winds to the springtime circulation along Monterey Bay's northern coastline. The phase between LML and the alongshore first modes was slightly positive, indicating that a positive alongshore (northwestward) current fluctuation follows a positive alongshore wind fluctuation, or wind relaxation (Fig. 15). Note this phase was significantly different from zero at just a few frequencies. This alongshore current variability is consistent with a simple, two-dimensional conceptualization of upwelling, although the mean flow is clearly not consistent with two-dimensional dynamics alone (Sections 3.1 and 3.2.).

A complex wind–current interaction at SHB during spring is revealed in Fig. 13: the highest wind-vs.-alongshore current coherence was found vs. the LML wind at periods of 2–9 days, but the highest wind-vs.-cross-shore current coherence was found against N42 winds at periods of 3–18 days. The difference in cross-shore coherences (N42 vs. SHB *u* 1st > LML vs. SHB *u* 1st) was statistically significant at periods of 5–18 days during spring, but the coherences were almost identical during winter (Fig. 14). Note the correspondence between the peak in winter coherence near 2–5 days and the peaks in wind and cross-shore power at the same periods (Fig. 10). In fall, SHB *u* 1st was not significantly coherent with

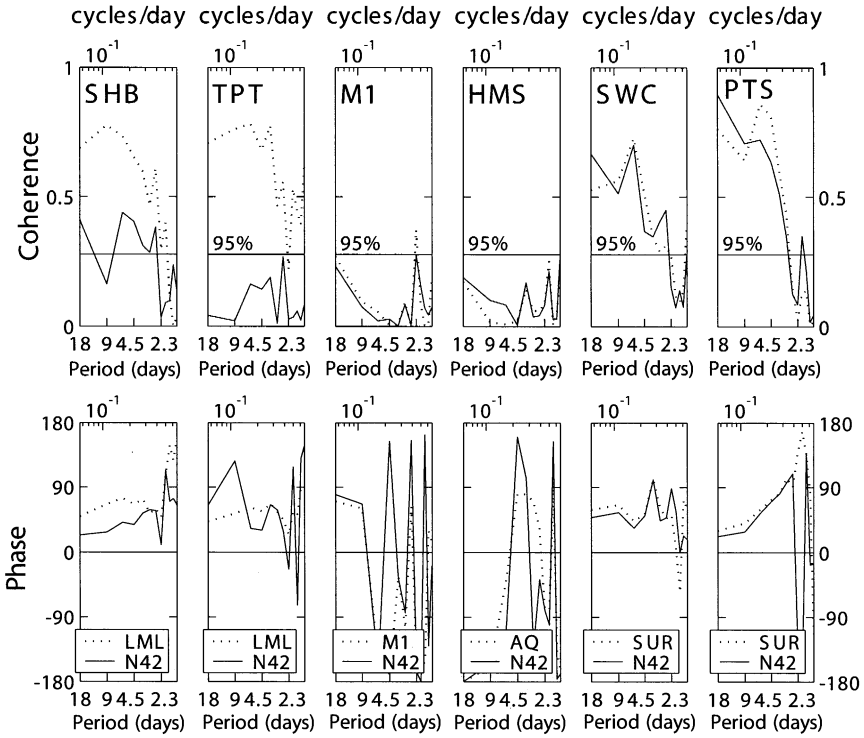

Fig. 9. Springtime wind vs. top temperature coherence, as in Fig. 7, but for springtime top temperatures.

LML winds, but did show significant coherence with N42 at periods of 9–18 days (not shown). The TPT cross-shore first mode was only significantly coherent with winds during spring and showed its highest coherence with LML. The phase between winds and cross-shore modes was slightly positive in spring and both positive and negative in winter, depending on the wind–current pairing, but was nowhere significantly different from zero. The coherence, phasing, vertical structure and relative size of the mode shapes indicate a straightforward cross-shore wind response: Positive (northwestward) wind fluctuations induce onshore current fluctuations near-surface and offshore fluctuations near-bottom, with no significant lag (Fig. 15). Conversely, southward (upwelling favorable) wind fluctuations result in offshore fluctuations near-surface and onshore flow near-bottom. This is again consistent with a classical picture of upwelling and Ekman dynamics, with equatorward winds driving offshore flow in the surface layer, resulting in compensatory onshore flow at depth. At SHB, cross-shore currents exhibited this pattern all three seasons, but at TPT the process was limited to spring.

4. Summary

During 2001 and 2002, inner shelf temperatures in the Monterey Bay area showed an annual cycle and general seasonality consistent with earlier observations from within Monterey Bay (Graham and Largier, 1997) and mid-shelf observations from the central and northern California coast (Largier et al., 1993; Strub et al., 1987). The seasonal wind behavior, measured at numerous stations, was also consistent with previous measurements (Halliwell and Allen, 1987). However, the annual cycle of inner shelf currents near the

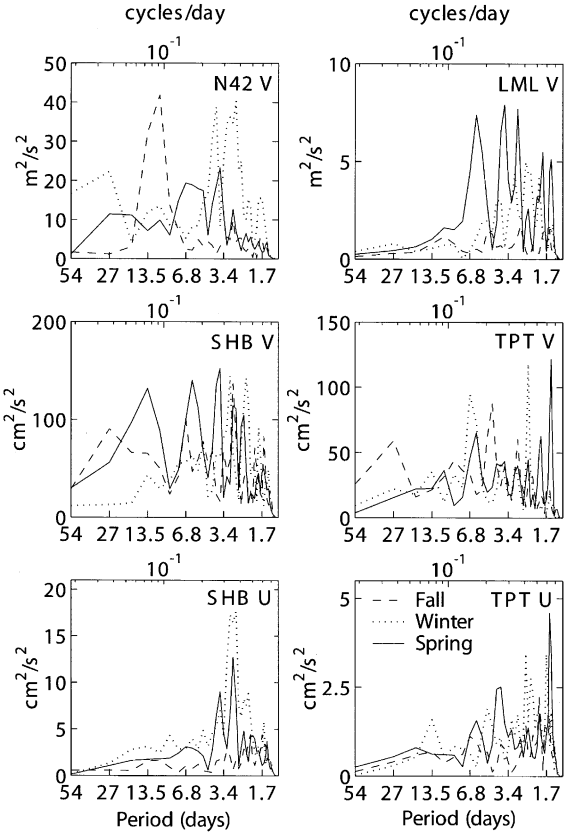

Fig. 10. Wind and current spectral shapes for each season, in variance-preserving form. The top two panes are the same as Fig. 5. Wind and current components are alongshore (v) and cross-shore (u). Measurement depths were 2 m at SHB and 3 m at TPT for all seasons. Only one depth is shown.

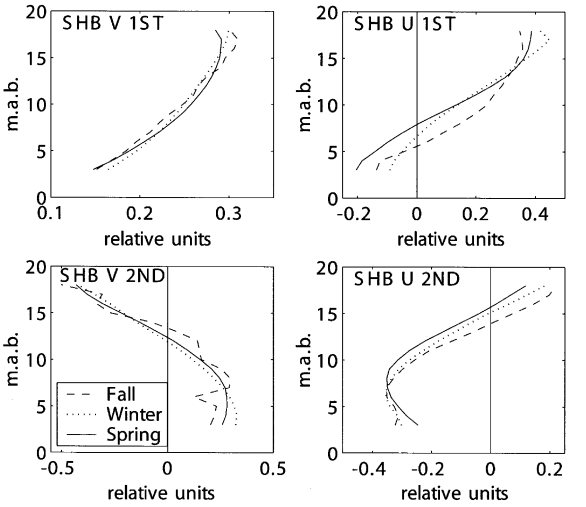

Fig. 11. SHB EOFs, or mode shapes, calculated separately for each velocity component and each season. Each mode represents a coherent current fluctuation moving in-phase throughout the water column. The relative strength of the fluctuations is determined by the modal amplitudes (see text). The values are dimensionless.

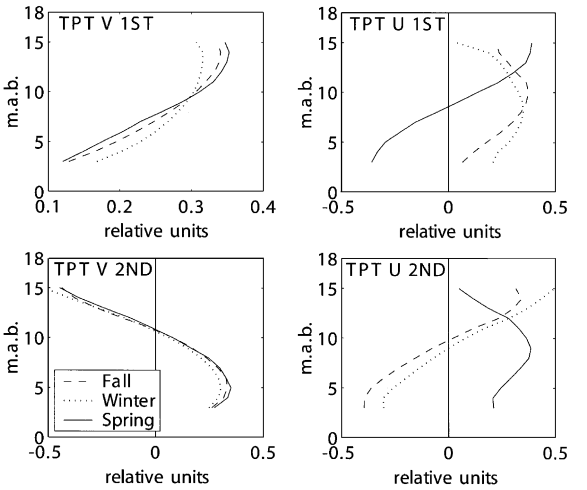

Fig. 12. TPT EOFs, or mode shapes, calculated for each velocity component and season.

bay's northern shore was markedly different from prior long-term observations on the northern California shelf. Currents were approximately out of phase with the annual wind signal, with currents flowing northwestward during both spring and fall, in direct opposition to the southeastward wind stress. Both winds and currents relaxed during winter, with currents approaching a near-zero mean. In the cross-shore momentum equation, mean alongshore currents, when northwestward, were apparently in geostrophic balance with a deduced cross-shore pressure gradient. However, the alongshore balance was not geostrophic. During spring and fall, a large alongshore barotropic pressure gradient was inferred in the alongshore momentum equation, balancing the combination of the southeastward wind stress and

the baroclinic pressure gradient. During these seasons, cross-shore mean vertical velocity profiles were similar to those from upwelling areas with poleward subsurface flow, showing offshore near-surface flow and a compensatory zone of onshore flow at mid-depth.

Remote wind forcing was of secondary importance to local currents and temperatures, if present at all. Considered annually, temperatures were coherent across the domain at periods of 15–60 days and coherent with local winds over the same frequency band. There were distinct differences in the temperature response to winds between seasons and sites. Sites south of Monterey Bay showed the highest year-round wind–temperature coherence, with the highest wind response found in spring and fall. Sites near the bay's northern shore showed the highest wind–temperature coherence during spring vs. a local land-based wind station. This wind station (LML) showed comparatively little correlation to the regional wind field. Alongshore currents in and near the northern bay were most coherent with winds in spring, and were also found to be most coherent with LML. Cross-shore currents displayed a more complex response to winds. Temperatures, alongshore currents and cross-shore currents all fluctuated with winds in a manner consistent with a two-dimensional conceptualization of upwelling. Wind relaxations were positively correlated with coastal warming, northwestward alongshore velocity fluctuations, onshore flow near-surface and offshore flow at depth.

Table 9
Current modal variance

Mode	Percent variance explained		
	Fall	Winter	Spring
SHB *v* 1st	84	96	96
TPT *v* 1st	97	95	93
SHB *v* 2nd	4.3	3.7	3.5
TPT *v* 2nd	2.8	3.8	5.2
SHB *u* 1st	40	67	61
TPT *u* 1st	56	57	53
SHB *u* 2nd	37	26	28
TPT *u* 2nd	31	31	36

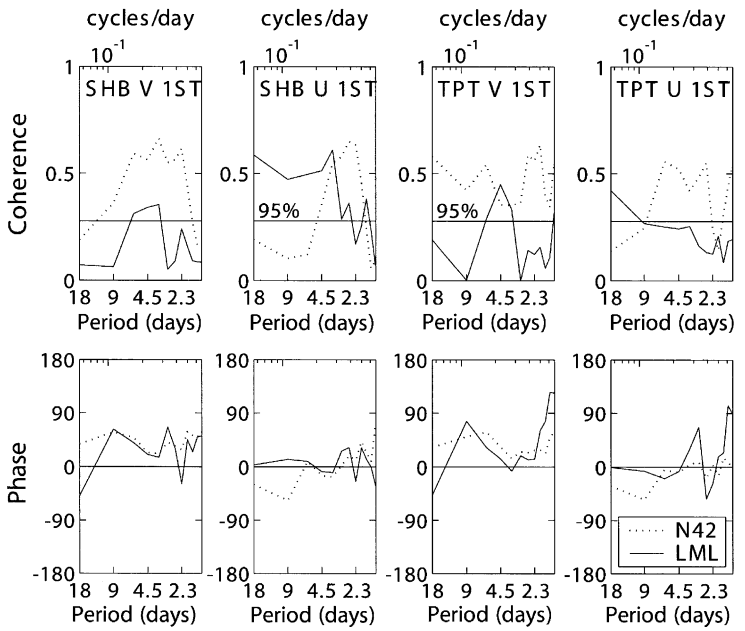

Fig. 13. Coherence of alongshore winds and first modes shape amplitudes during spring. Horizontal line is the value where coherence becomes statistically significant from zero to the 95% confidence level. Positive phase indicates that currents follow the wind.

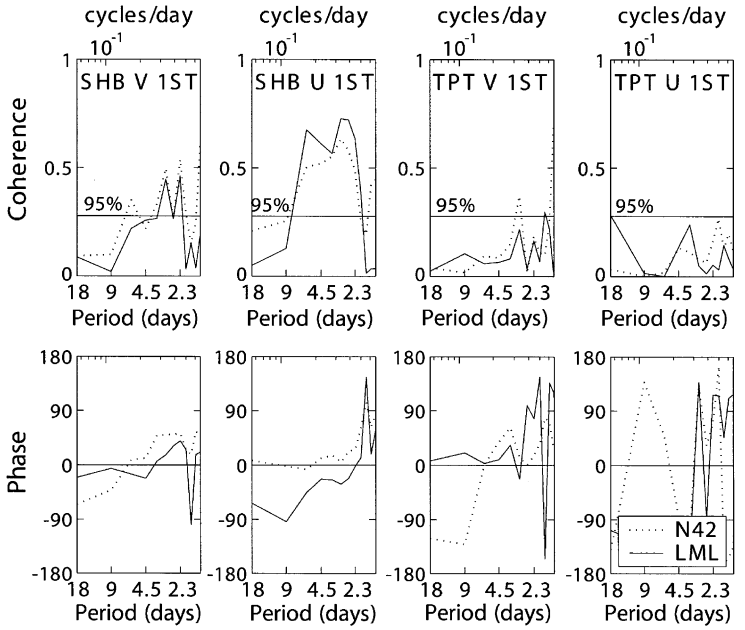

Fig. 14. Coherence of winds and first mode shapes during winter. Compare with Fig. 13 and SHB cross-shore power spectra, Fig. 10.

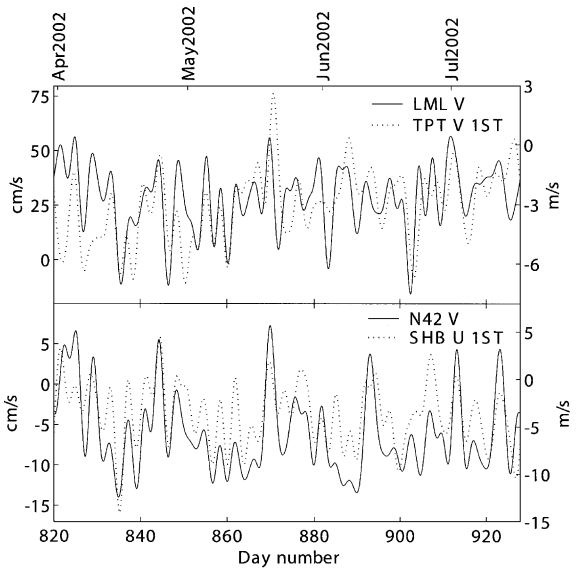

Fig. 15. Time histories of winds and TPT alongshore first mode amplitude (top panel) and SHB cross-shore first mode amplitude (bottom panel). In this figure only, data was low-passed with a half-power period of 3 days for display purposes. Monthly tick marks (top *x*-axis) fall on the first of the month.

Acknowledgments

The authors would like to thank Professors Mark Carr and Pete Raimondi of the University of California, Santa Cruz, for encouraging this research. Special appreciation is given to Jared Figurski and Jamie Grover of the UCSC PISCO group who performed much of the field work needed to obtain the PISCO data used here. Other thanks go to Dr. Chris Edwards at UCSC for his insights in developing this paper and an anonymous reviewer for his suggestions in simplifying the discussion of the alongshore pressure gradient. The Monterey Bay Aquarium, MBARI and the Department of Meteorology at the Naval Postgraduate School are also recognized for their generous contributions of wind and/or temperature data. This is contribution number 149 from PISCO, the Partnership for Interdisciplinary Studies of Coastal Oceans: a long-term ecological consortium funded by the David and Lucile Packard Foundation.

References

Allen, J.S., 1975. Coastal trapped waves in a stratified ocean. Journal of Physical Oceanography 5, 300–325.

Bendat, J.S., Piersol, A.G., 2000. Random Data. Wiley, New York (594pp).

Breaker, L.C., Broenkow, W.W., 1994. The circulation of Monterey Bay and related processes. Oceanography and Marine Biology: An Annual Review 32, 1–64.

Chelton, D.B., Bratkovich, A.W., Bernstein, R.L., Kosro, P.M., 1988. Poleward flow off central California during the spring and summer of 1981 and 1984. Journal of Geophysical Research 93 (C9), 10,604–10,620.

Davis, R.E., Bogden, P.S., 1989. Variability on the California shelf forced by local and remote winds during the coastal ocean dynamics experiment. Journal of Geophysical Research 94 (C4), 4763–4783.

Denbo, D.W., Allen, J.S., 1987. Large-scale response to atmospheric forcing of shelf currents and coastal sea level off the West Coast of North America: May–July 1981 and 1982. Journal of Geophysical Research 92 (C2), 1757–1782.

Emery, W.J., Thomson, R.E., 1997. Data Analysis Methods in Physical Oceanography. Elsevier, New York (634pp).

Graham, W.M., Largier, J.L., 1997. Upwelling shadows as nearshore retention sites: the example of northern Monterey Bay. Continental Shelf Research 17 (5), 509–532.

Halliwell Jr., G.R., Allen, J.S., 1987. The large-scale coastal wind field along the West Coast of North America, 1981–1982. Journal of Geophysical Research 92 (C2), 1861–1884.

Harris, F.J., 1978. On the use of windows for harmonic analysis with the discrete Fourier transform. Proceedings of the IEEE 66, 51–83.

Huyer, A., 1983. Coastal upwelling in the California current system. Progress in Oceanography 12, 259–284.

Kosro, P.M., Huyer, A., Ramp, S.R., Smith, R.L., Chavez, F.P., Cowles, T.J., Abbott, M.R., Strub, P.T., Barber, R.T., Jessen, P., Small, L.F., 1991. The structure of the transition zone between coastal waters and the open ocean off Northern California, winter and spring 1987. Journal of Geophysical Research 96 (C8), 14,707–14,730.

Kundu, P.K., Allen, J.S., 1976. Some three-dimensional characteristics of low-frequency current fluctuations near the Oregon Coast. Journal of Physical Oceanography 6, 181–199.

Kundu, P.K., Allen, J.S., Smith, R.L., 1975. Modal decomposition of the velocity field near the Oregon Coast. Journal of Physical Oceanography 5, 683–704.

Large, W.G., Pond, S., 1981. Open ocean momentum flux measurements in moderate to strong winds. Journal of Physical Oceanography 11, 324–336.

Largier, J.L., Magnell, B.A., Winant, C.D., 1993. Subtidal circulation over the Northern California Shelf. Journal of Geophysical Research 98 (C10), 18,147–18,179.

Lentz, S.J., 1987. A description of the 1981 and 1982 spring transitions over the Northern California Shelf. Journal of Geophysical Research 92 (C2), 1545–1567.

Lentz, S.J., 1994. Current dynamics over the Northern California Shelf. Journal of Physical Oceanography 24, 2461–2478.

Lentz, S., Trowbridge, J., 2001. A dynamical description of fall and winter mean current profiles over the Northern California Shelf. Journal of Physical Oceanography 31, 914–931.

Paduan, J.D., Rosenfeld, L.K., 1996. Remotely sensed surface currents in Monterey Bay from shore-based HF radar (Coastal Ocean Dynamics Radar). Journal of Geophysical Research 101 (C9), 20,669–20,686.

Pringle, P.M., Riser, K., 2003. Remotely forced nearshore upwelling in Southern California. Journal of Geophysical Research 108 (C4), 3131.

Ramp, S.R., Abbott, C.L., 1998. The vertical structure of currents over the Continental Shelf off point Sur, CA, during spring 1990. Deep Sea Research II 45, 1443–1470.

Smith, R.L., 1981. A comparison of the structure and variability of the flow field in three coastal upwelling regions: Oregon, Northwest Africa, and Peru. In: Richards, F.A. (Ed.), Coastal Upwelling, Coastal and Estuarine Science, vol. 1. AGU, Washington, DC, pp. 107–118.

Storlazzi, C.D., McManus, M.A., Figurski, J.D., 2003. Long-term, high-frequency current and temperature measurements along central California: insights into upwelling/relaxation and internal waves on the inner shelf. Continental Shelf Research 23 (9), 901–918.

Strub, P.T., Allen, J.S., Huyer, A., Smith, R.L., 1987. Seasonal cycles of currents, temperatures, winds, and sea level over the Northeast Pacific Continental Shelf: 35°N to 48°N. Journal of Geophysical Research 92 (C2), 1507–1526.

Thompson, R.O.R.Y., 1979. Coherence significance levels. Journal of the Atmospheric Sciences 36, 2020–2021.

Winant, C.D., Beardsley, R.C., Davis, R.E., 1987. Moored wind, temperature, and current observations made during coastal ocean dynamics experiments 1 and 2 Over Northern California continental shelf and upper slope. Journal of Geophysical Research 92 (C2), 1569–1604.